Optics Letters

Swept-source optical coherence tomography microsystem with an integrated Mirau interferometer and electrothermal micro-scanner

P. Struk,[1,2] S. Bargiel,[1] Q. A. A. Tanguy,[1] F. E. Garcia Ramirez,[1] N. Passilly,[1] P. Lutz,[1] O. Gaiffe,[1] H. Xie,[3] and C. Gorecki[1,*]

[1]FEMTO-ST Institute (UMR CNRS 6714), UBFC, 15B Avenue des Montboucons, 25030 Besançon cedex, France
[2]Silesian University of Technology, 2 Akademicka Str., 44-100 Gliwice, Poland
[3]University of Florida, P.O. Box 116200, Gainesville, Florida 32611-6200, USA
*Corresponding author: christophe.gorecki@femto-st.fr

Received 19 June 2018; revised 24 August 2018; accepted 24 August 2018; posted 6 September 2018 (Doc. ID 335148); published 1 October 2018

In the rapid evolution of gastrointestinal endomicroscopy, optical coherence tomography (OCT) has found many diverse applications. Until recently, the micro-opto–electro-mechanical systems (MOEMS) technology has been playing a key role in shaping the miniaturization of these components. We report here, to the best of our knowledge, a novel endoscopic microsystem. It is based on a spectrally tuned MOEMS Mirau micro-interferometer integrated with micro-electro-mechanical systems (MEMS) electro-thermal micro-scanner, operating in the regime of swept-source (SS) OCT imaging. This Letter validates our initial proof-of-concept toward the development of such MOEMS probe and the presentation of experimental performances of the resulting SS-OCT microsystem.

https://doi.org/10.1364/OL.43.004847

With the development of micro-electro-mechanical systems (MEMS) and micro-opto–electro-mechanical systems (MOEMS) technologies, a wide variety of movable and tunable mirrors, lenses, filters, and other optical structures has been proposed [1]. Those components are useful in building of optical-fiber-based endoscomicroscopes with great potentials for clinical translation: optical coherence tomography (OCT) [2], confocal microscopy [3], and photoacoustic or multiphoton microscopies [4,5]. Endomicroscopes are adapted to provide *in vivo* real-time imaging with cellular resolutions, approaching those of conventional microscopy techniques. The cost effectiveness of all these endomicroscopes permits portability, therefore increasing the usability and serviceability of medical instruments. Also, an increasing demand for the reduction of sizes, as well as lower cost, has made in particular the miniaturization of interferometric systems an important issue. One of the OCT approaches that can benefit from the significant improvement in equipment efficiency and quality of medical diagnosis made by incorporating MOEMS technology is the swept-source OCT (SS-OCT). It allows a fast and non-invasive 3D reconstruction of tissue morphology within a significant penetration depth (~1.5 mm) and high resolution (5–10 μm). Compared with other OCT techniques, SS-OCT offers higher sensitivity and faster axial scanning, leading to the reduction of the motion artifacts [6]. Various MOEMS-based OCT probes, typically based on hybrid integration of beam-shaping optics with miniature scanning engines (e.g., 2D scanning micromirrors, movable/tunable microlenses), have been demonstrated [7,8]. Besides the probe, further miniaturization of SS-OCT systems is possible by replacing its core component—the Michelson interferometer by interferometry configurations with a better potential of miniaturization. The interest of such a approach has been demonstrated recently for a miniature 5 × 5 array of low-coherence Mirau micro-interferometers [9]. Thus, the entire active array of Mirau interferometers can be stacked using a multi-wafer vertical integration method [10]. We propose here a passive Mirau micro-interferometer, well suited to be vertically integrated by micromachining [11]. The Mirau architecture also simplifies the OCT setup and makes it insensitive to the small path-length differences, caused by probe change or by the influence of environment (fiber bending, temperature).

This Letter, to the best of our knowledge, presents an original architecture of an SS-OCT microsystem based on a spectrally tuned single-channel Mirau micro-interferometer, integrated with a MEMS electro-thermal micro-scanner. We focus on the design, technology, and characterization of the SS-OCT microsystem main blocs, followed by a discussion of optical and imaging performances.

Figure 1 shows the main blocks of the SS-OCT microsystem:

– the core of OCT device, a MOEMS probe connected to the illumination/detection blocks by single-mode optical fiber. This includes a Mirau micro-interferometer with a MEMS micro-scanner moving around the position inclined at 45° from the optical axis;

– the illumination block including a tunable laser swept source (ESS-840 Exalos) with a central wavelength $\lambda_c = 840$ nm

and a swept range $\Delta\lambda = 60$ nm, A-scan frequency of 110 kHz, and an optical fiber circuit with an optical circulator (Fibrain);

– the detection block including a single point detector (PDB430A Thorlabs), the k-clock generating a reference signal used for k-space resampling during post-processing of OCT image, the data acquisition card (1250X GaGe CompuScope digitizer board, GaGe, 500 MS/s per channel, 12-bit resolution), and PC control unit. The SS-OCT endomicroscope of Fig. 1 can work in two different modes: (i) a transverse scanning mode with the micro-scanner integrated on top of Mirau interferometer where the dashed line in the figure represents the light beam deflected by MEMS actuator; and (ii) a forward scanning mode without the microscanner deflecting the beam where the probing beam is focused directly on the sample—the beam is here represented by the solid line. In this last regime, the scanning needs to be performed with help of an external 3D motorized stage.

The detailed process flow, as well as the characterization of components of the Mirau interferometer, are given in Ref. [11]. The role of a gradient-index (GRIN) lens collimator is to generate a collimated light beam with a diameter of 1 mm, which illuminates a plano-convex glass lens (1.9 mm in diameter) of the Mirau micro-interferometer. The convergent light beam is afterward divided by the beam-splitting plate (BSP) into a reference beam and a scanning beam. The BSP is made of a thin-film of a TiO_2 layer deposited on the Borofloat 33 glass. A silicon separator ensures the position of the BSP at half of the focal length of the focusing lens (focal length of 9 mm). The reference beam is back-reflected from the reference micromirror (diameter of 150 μm), made of Ti/Ni/Au layers at the backside of the focusing lens, whereas the scanning beam is directed by the two-axis MEMS scanner toward the sample (side-viewing probe). The axial resolution of the probe of 5.2 μm is determined by the central wavelength and the swept range of the laser source. The transverse resolution is defined by the effective numerical aperture (NA = 0.055) of the focusing lens, and it is limited to 9.8 μm. Figure 2(a) shows the cross-section of monolithically integrated Mirau micro-interferometer, including silicon base for the GRIN lens assembly port (1) and glass wafer with reflowed focusing lens, containing the reference micromirror (2), silicon separator (3), and beam splitter plate (4).

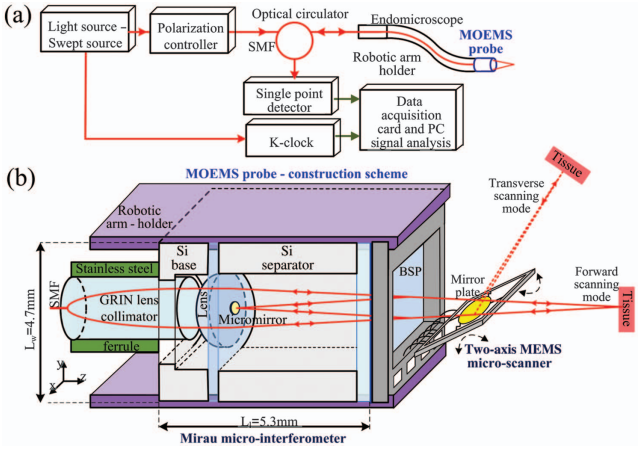

Fig. 1. SS-OCT endomicroscope: (a) schematic of SS-OCT microsystem; (b) zoom on the MOEMS probe.

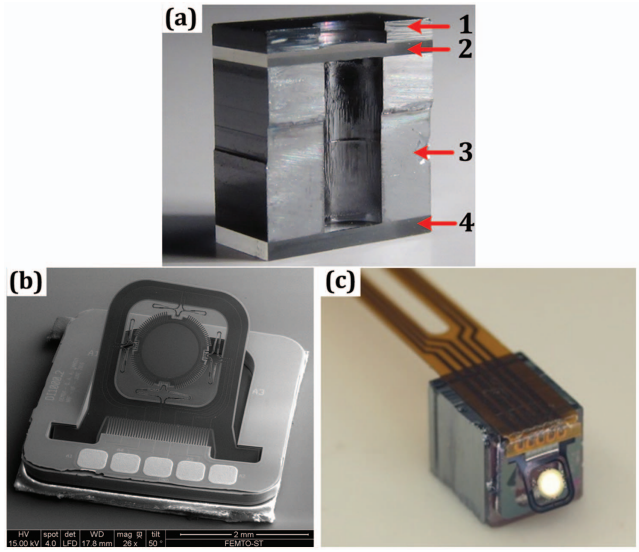

Fig. 2. Building blocks and assembly of the OCT probe: (a) vertical cross section of the Mirau micro-interferometer; (b) view of the electrothermal two-axis micro-scanner with a mechanical stopper; and (c) final chip of assembled MOEMS probe with electrical contacts.

The probe is intended to be attached to a continuum robotic arm [12], installed at the distal end of the endomicroscope, positioning continuously the probe during the side scanning of the specimen. The k-clock used during the post-processing data analysis (k-space resampling) is acquired using a Mach–Zehnder interferometer (INT-MZI-850, Thorlabs). The sensitivity of presented probe is approximately 80–90 dB. The detailed analysis of sensitivity, noises, optical power budget, losses, and axial and transverse resolutions is presented in Ref. [11]. The specifications of the Mirau interferometer are listed in Table 1.

The principle of operation, technology, and characterization of two-axis micro-scanner are detailed in Ref. [13], while the design of the micromirror version including the mechanical stopper is described in Ref. [14]. The micro-scanner allows the extension of the swept area by scanning two additional directions (B-scans), which are orthogonal to the swept source A-scan axis. Thus, a 3D image is reconstructed by scanning the focused beam, deflected perpendicularly toward the sample and the backscattered light back into the interferometric block. The scanning device is fabricated onto a silicon on insulator (SOI) wafer using electrothermal actuators to enable the uncoupled motion of the central mirror plate over two orthogonal axes. The microactuators are composed of bimorphs made of Al/SiO_2 layers, providing large angular displacements (up to $\pm 22°$) at high frequencies (>1 kHz) for low voltages (<20 V). Figure 2(b) shows the two-axis MEMS micro-scanner including

Table 1. Specifications of the Mirau-Based SS-OCT Probe

Lens Focal Length	Lens Radius Curvature	Sag of Lens	Axial Resolution	Transverse Resolution
9.0 mm	4.19 mm	109 μm	5.2 μm	9.8 μm

the stopper maintaining the position of the mirror inclined at 45° from the optical axis.

The assembly of the MOEMS probe is based on the vertical integration of the electrothermal micro-scanner on top of the monolithic Mirau micro-interferometer. The building components have been hybridly integrated at the chip-level, mainly due to the current out-of-plane position of the scanning micromirror after releasing. All assembly steps were performed using a semi-automatic chip-bonder tool (HB70, TPT), equipped with electrically heated vacuum stage with precise X–Y displacement capability. The alignment of the structures was made using a high-resolution camera with an adjustable viewing angle. First, the scanner chip was positioned and sealed by adhesive bonding onto the Mirau micro-interferometer. Before the assembly of the flexible printed circuit board (PCB), small dots of electrically conductive silver epoxy (Epotec, H20e) were deposited by the stamping method on the contact pads of the micro-scanner, and next, the bonded structure of the Mirau interferometer with the micro-scanner was positioned horizontally. After the alignment and contact of the PCB pads with the pads of the micro-scanner, the chuck was heated to cure the epoxy glue. Figure 2(c) shows the assembled version of the MOEMS probe.

Three experiments were performed to validate the optical performances of the SS-OCT microsystem: the evaluation of transverse resolution, the evaluation of the reproducibility of the micro-scanner scanning, and the OCT imaging performances.

First, the transverse resolution of the Mirau micro-interferometer, estimated theoretically to be 9.63 μm [11], has been confirmed experimentally using the chrome-on-glass USAF 1951 resolution test target (defined by the U.S. Air Force MIL-S-150A standard of 1951). The test bars of Group 5 were scanned, as shown in Fig. 3. The bright areas of the picture represent places where the metal layer is present, while the dark area corresponds to the glass layer. The width of individual bars on the scanned USAF target is marked on the picture by arrows. Most of the test bars of Group 5 are well visible. The estimated value of transverse resolution is 9.84 μm, matching the theoretical value. The camera is said to "resolve" a chart element, if the vertical and horizontal bars can still be recognized as three distinct bars and do not blur into one another.

Second, scan trajectories based on Lissajous curves have been studied by laser scan of a small reflective surface (770 × 270 μm^2) at the resonant frequency of a micro-scanner mirror. The goal here is to evaluate the repeatability of the scan for a further characterization of the fully integrated microsystem. The real output of a Lissajous scan, performed at the resonance frequencies of each axis, was sufficiently stable to be compensated by a rectification model including the non-random thermal, geometrical, and other nonlinear effects. The scanned surface was covered at 99% with a laser spot size

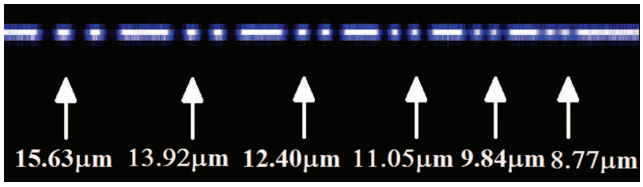

Fig. 3. Transverse resolution of SS-OCT probe (USAF 1951 resolution test target).

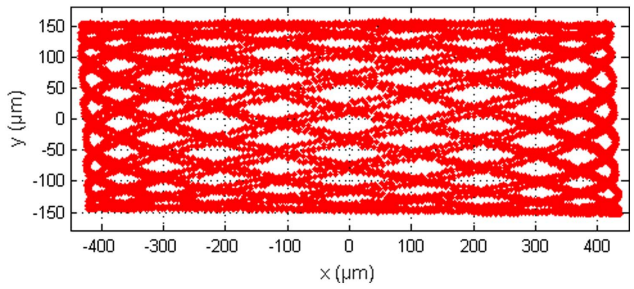

Fig. 4. Time-elapsed Lissajous scanning patterns with a field-of-view of 770 × 270 μm^2 after 200 ms.

of 20 μm within a real-time acquisition, as shown in Fig. 4. The standard deviation between the predicted output and the real position is less than 0.051° for a mean absolute error of 0.011°, which corresponds to less than the resolution of the optical system. However, these results were not exploited for the final imaging yet, and they are presented here to underline the future potential of the integrated SS-OCT probe.

Third, we acquired series of 3D cross-sectional images (B-scans) of a specific test sample. Such B-scans are created by laterally scanning the OCT beam and collecting sequential A-scans. Here, the A-scan rate is determined by the sweep speed of the swept laser source. The test sample ensures the optical contrast between layers with defined refractive indexes as well as thickness of each layer. Proposed test sample is built in the form of 30-μm-thick SU-8 resist ($n = 1.58$ at 840 nm) disc with a 2 mm diameter, separated by a 20-μm-wide trench. The SU-8 discs are covered by a 20-μm-thick spray-coated S1813 photoresist ($n = 1.62$ at 840 nm). The photoresist layers were deposited on 0.5-mm-thick Borofloat 33 glass ($n = 1.465$ at 840 nm). Figure 5(a) shows the cross-section and a picture of the test sample.

The OCT image from our SS-OCT microsystem was compared with the images from a commercial system, the spectral-domain OCT Telesto from Thorlabs. Figure 5(b) shows the B-scan of our test sample, obtained by Telesto system. This represents interfaces where the refractive index changes. The length of B-scan (8 mm) is here close to the

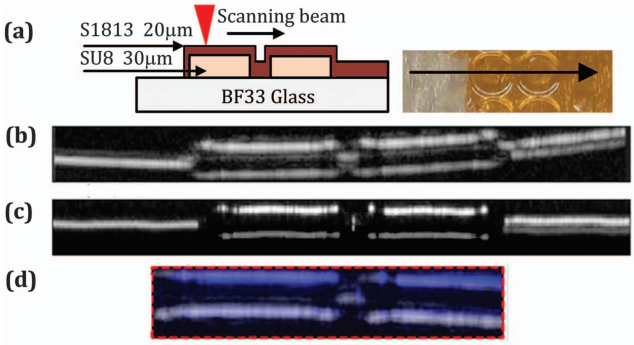

Fig. 5. Test sample and the comparison of OCT B-scans: (a) cross-section of a multilayer test sample and image of the test sample with the direction of B-scan; (b) B-scan of the test sample obtained by Thorlabs Telesto; (c) B-scan of the test sample obtained by the SS-OCT MOEMS probe; and (d) superimposition of (b) and (c) B-scans in different color bands.

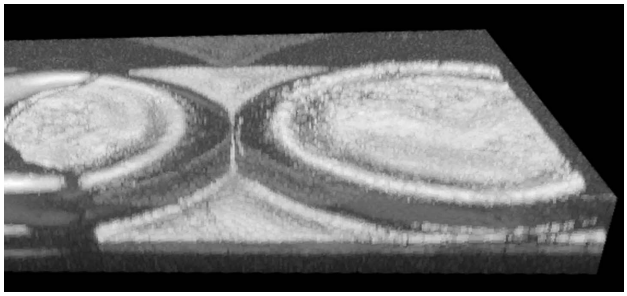

Fig. 6. 3D-perspective OCT image of the test sample where an area of 3.5×2 mm^2 is exploited.

lateral dimension of the field-of-view of Telesto objective (10×10 mm^2). The slight curvature of B-scan is produced here by a scanning method where the scanning beam is reflected by a galvanometric mirror. To cover the complete area of the field-of-view of the OCT head, the galvanometric mirror increases the scanning distance between the central part and external part of the sample, introducing the curvature effect in the RAW OCT image. Figure 5(c) shows the B-scan of our test sample measured with the SS-OCT MOEMS probe. This result is obtained in absence of the micro-scanner by forward scanning mode of Fig. 1(b). Here, the test sample was placed perpendicularly to the front side of the MOEMS probe fixed on a translation stage performing the lateral scanning with the step of 5 μm (1 mm of B-scan includes 200 A-scans). The B-scan image from our OCT microsystem is comparable to that from the commercial system. Successive interfaces where the refractive index of photoresist changes can be seen: the BF33 glass, the double layer of photoresist with a thickness of 50 μm, the small gap between the pattern on glass in the form of a single layer of photoresist of 20 μm, the double layer of photoresist 50 μm thick, and a single layer of photoresist 20 μm thick.

In Fig. 5(d) the central parts of the two B-scan curves were superimposed on each other, demonstrating that the measured axial resolutions of both instruments are well comparable. The B-scans are presented in different color bands: the MOEMS probe result is in blue, and the Telesto result is in gray. Figure 6 shows the 3D perspective OCT image of the sample where the depth of the image is 126 μm, and the dynamic range is approximately 50 to 55 dB.

We reviewed the experimental results of, to the best of our knowledge, a novel SS-OCT microsystem including a miniature Mirau-based interferometer coupled with a two-axis MEMS electrothermal scanner, demonstrating experimentally the prove-of-concept of this approach. The small size of the endomicroscope, combined with the high-resolution of interferometry and the precise alignment of the MEMS scanner, comes with miniaturization and makes this MOEMS probe well suited to be incorporated into the optical endoscopes that are going to be used in future clinical applications. Focusing microlens surfaces of MOEMS probe are not covered by AR coating, resulting in a power loss up to 10 dB. It is essential now to solve the challenges derived from the assembly of MEMS and MOEMS components, which could introduce image artifacts or distortions. The next steps of development will include a successful integration of the endomicroscope on top of the robotic arm, as well as the improvements of optical quality of Mirau components, such as the deposition of AR coatings.

Funding. Centre National de la Recherche Scientifique (CNRS); Agence Nationale de la Recherche (ANR) (ANR-11-LABX-0001-01).

Acknowledgment. This work was supported by the Labex Action program, the French RENATECH network and its FEMTO-ST technological facility and by the Collegium SMYLE. We thank Jean Marc Cote for his help in the development of acquisition and image-processing software.

REFERENCES

1. O. Solgaard, A. A. Godil, R. T. Howe, L. P. Lee, Y. A. Peter, and H. Zappe, J. Microelectromechan. Syst. **23**, 517 (2014).
2. Z. Qiu and W. Piyawattanamatha, Micromachines **8**, 210 (2017).
3. J. B. Pawley, ed., *Handbook of Biological Confocal Microscopy*, 3rd ed. (Springer, 2006).
4. W. Denk, J. H. Strickler, and W. W. Webb, Science **248**, 73 (1990).
5. H. Fritjof and W. Denk, Nat. Methods **2**, 932 (2005).
6. W. Dexler, M. Liu, A. Kumar, T. Kamali, A. Unterhuber, and R. Leitgeb, J. Biomed. Opt. **19**, 071412 (2014).
7. C. Duan, X. Zhang, D. Wang, Z. Zhou, P. Liang, A. Pozzi, and H. Xie, *IEEE 11th International Symposium on Biomedical Imaging (ISBI)* (2014), pp. 1397–1400.
8. J. Sun and H. Xie, Int. J. Opt. **2011**, 1 (2011).
9. J. Albero, S. Bargiel, N. Passilly, P. Dannberg, M. Stumpf, and U. D. Zeitner, J. Micromech. Microeng. **21**, 065005 (2011).
10. J. Lullin, S. Bargiel, P. Le Moal, S. Perrin, J. Albero, N. Passilly, L. Froehly, F. Lardet-Vieudrin, and C. Gorecki, J. Micromech. Microeng. **25**, 115013 (2015).
11. P. Struk, S. Bargiel, L. Froehly, M. Baranski, N. Passilly, J. Albero, and C. Gorecki, IEEE Sens. J. **15**, 7061 (2015).
12. M. Taha Chikhaoui, K. Rabenorosoa, and N. Andreff, Mech. Mach. Theory **104**, 234 (2016).
13. Q. A. A. Tanguy, S. Bargiel, H. Xie, N. Passilly, M. Barthès, O. Gaiffe, J. Rutkowski, P. Lutz, and C. Gorecki, Micromachines **8**, 146 (2017).
14. Q. A. A. Tanguy "Design and fabrication of a MEMS scanner for OCT imaging endo-microscopic probe," Ph.D. dissertation (Université de Franche-Comté, 2018).